Nanotechnology **20** (2009) 235705 (5pp) doi:10.1088/0957-4484/20/23/235705

Probing surface plasmons in individual Ag nanoparticles in the ultra-violet spectral regime

Ming-Wen Chu[1,6], Pradeep Sharma[2,3,4], Ching-Pin Chang[1,5], Sz Chian Liou[1], Kun-Tong Tsai[2], Juen-Kai Wang[1,2], Yuh-Lin Wang[2,4] and Cheng Hsuan Chen[1,2,4]

[1] Center for Condensed Matter Sciences, National Taiwan University, Taipei 106, Taiwan
[2] Institute of Atomic and Molecular Sciences, Academia Sinica, Taipei 106, Taiwan
[3] Taiwan International Graduate Program, Academia Sinica, Taipei 106, Taiwan
[4] Department of Physics, National Taiwan University, Taipei 106, Taiwan
[5] Department of Materials Science and Engineering, National Taiwan University, Taipei 106, Taiwan

E-mail: chumingwen@ntu.edu.tw

Received 20 January 2009, in final form 7 April 2009
Published 19 May 2009
Online at stacks.iop.org/Nano/20/235705

Abstract

Previous investigations of surface plasmons in Ag largely focused on their excitations in the visible spectral regime. Using scanning transmission electron microscopy with an electron beam of 0.2 nm in conjunction with electron energy-loss spectroscopy, we spectrally and spatially probe the surface plasmons in individual Ag nanoparticles (∼30 nm), grown on Si, in the ultra-violet spectral regime. The nanomaterials show respective sharp and broad surface-plasmon resonances at ∼3.5 eV (∼355 nm) and ∼7.0 eV (∼177 nm), and the correlated spectral calculations established their multipolar characteristics. The near-field distributions of the surface plasmons on the nanoparticles were also mapped out, revealing the predominant dipolar nature of the 3.5 eV excitation with obvious near-field enhancements at one end of the nano-object. The unveiled near-field enhancements have potential applications in plasmonics and molecular sensing.

(Some figures in this article are in colour only in the electronic version)

1. Introduction

Surface plasmons (SPs) are quantized collective plasma oscillations of conduction electrons propagating at the surface of metals [1–10]. The excitations of SPs by the dipolar electric field of light in the visible spectral regime dictate the color of noble metals [4].

In noble metal nanoparticles (NPs) with sizes of only a few tens or hundreds of nanometers, SPs tailored by the sizes, shapes, and electric near-field couplings of the NPs determine their optical properties ranging from near-infrared to visible spectral regimes, as demonstrated in nanoprisms [8], nanorings [9], nanostars [10], (coupled) nanorods [5, 11], and (coupled/arrayed-) nanospheres [6, 12–16]. In individual and/or coupled NPs with designated geometrical constraints, SPs can then be tuned to the proximity of the laser energies/wavelengths conventionally available [17]. The associated excitations have been shown to open up vast opportunities for many fascinating applications of the NPs such as plasmonics [17, 18] and molecular sensing by surface enhanced Raman scattering (SERS) [13, 19]. It has been noted that these novel applications are closely correlated with the SP characteristic and the correlated near-field distributions in each individual nanomaterial [6, 10, 17]. The corresponding spectral characterization requires spectroscopy techniques with a nanometer-scale spatial resolution that is, however, difficult to achieve by optical approaches, even by advanced nanoprobe-based scanning near-field optical microscopy (SNOM) [20].

[6] Author to whom any correspondence should be addressed.

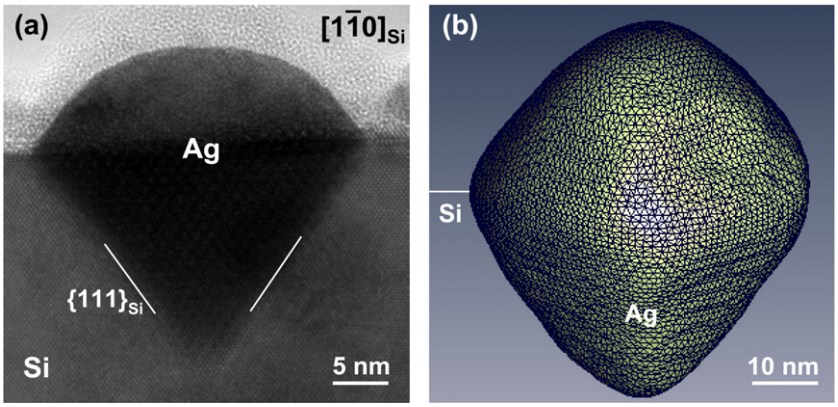

Figure 1. (a) TEM image of an individual Ag NP grown on Si(100). The image was acquired along the $[1\bar{1}0]_{Si}$ projection. (b) Three-dimensional imaging of such an individual Ag NP using STEM electron tomography.

An electron beam can excite SPs like light by coupling its electromagnetic field to the evanescent electric fields of SPs, and the corresponding excitations are manifested by electron energy losses at the given SP eigen-frequencies [21, 22]. The sub-nanometer electron beam in a scanning transmission electron microscope (STEM) and the appreciable kinetic energy of the incident electrons (a few hundreds of kV) thus provide the unmatched spatial resolution and energy range in spectrally and spatially studying the SPs in individual NPs, when used in conjunction with electron energy-loss spectroscopy (EELS), STEM-EELS [8, 21, 23]. Using STEM-EELS, the spatially resolved probing of SPs in individual Ag nanoprisms [8] and individual and coupled Au NPs [23] in the visible spectral regime has been demonstrated.

Here, we address the experimental and theoretical aspects of SPs in individual Ag NPs (∼30 nm) grown on Si(100) substrates in the ultra-violet spectral regime, for which conventional optical probing is marginal [21] and thus less well understood. All experimental results show good agreement with the associated STEM-EELS calculations [22, 24], and the spatial distributions of the surface excitations on the NPs were also unambiguously mapped out.

2. Experimental details

The STEM-EELS investigations of the Ag NPs were performed on a field-emission TEM/STEM, FEI Tecnai F20, operated at 200 kV and equipped with a Gatan Tridiem EELS spectrometer. The electron energy resolution (defined by the line-width of the zero-loss peak, ZLP) and beam size exploited throughout the work were ∼0.66 eV and ∼0.2 nm, respectively. Respective spectrum collection and probe convergence semi-angles of 4.9 and 13 mrad were used. The electron tomography was conducted on the sample microscope with the STEM Z-contrast images acquired in the sample-tilt range of ±60° and the corresponding three-dimensional reconstructions performed in the FEI Inspect3D package. The growth of the arrayed Ag NPs (size, ∼30 nm; gaps between NPs, ∼50 nm) by focused-ion-beam patterning of Si substrates and subsequent post-annealing of Ag films on the patterned substrates was reported in a separate work [25]. The Ag NPs/Si samples for STEM-EELS studies were prepared by standard mechanical and ion-milling thinning techniques and then subject to HF and repeated plasma cleanings before the investigations in order to improve the sample surface cleanness.

3. Results and discussion

Figure 1(a) illustrates the typical TEM image of an individual Ag NP among the arrays. The upper part of the NP in vacuum shows a hemisphere-like geometrical configuration, while the lower part embedded in Si is characterized by a V-shape groove defined by the {111} faces of Si [25]. On the surfaces of both Ag NP and Si (figure 1(a)), one can also observe residual thin amorphous contamination layers that, however, do not affect STEM-EELS investigations below. To confirm the shape feature of the Ag NPs, STEM electron tomography was performed on several NPs and figure 1(b) exhibits the corresponding three-dimensional image of an individual NP. From figure 1(b), it is obvious that the conventional specimen thinning does not flatten the NPs to two-dimensional thin-slab-like shapes as thinning usually does. In figure 1(b), the $\{111\}_{Si}$-type facets of the NPs (lower part) and the smoother hemisphere-like head (upper part) can also be clearly observed. These characteristics are essential for the following SP investigations considering the sensitivity of SP-excitation energies to geometrical constraints of Ag, such as ∼3.7 eV (∼335 nm) for thin Ag slab [26] and ∼3.5 eV (∼355 nm) for spherical and hemispherical Ag NPs [27].

Figure 2(a) shows the STEM-EELS spectra acquired at different locations of the Ag NP (black, red, green, and blue curves), and a spectrum at 1 nm from the Si surface and ∼20 nm from the edge of the NP was also taken (purple curve). It should be noted that the mean inter-particle gap spacing of ∼50 nm [25] is too large to exhibit any noticeable SP coupling between the Ag NPs (gaps of at most around ten nanometers are necessary for effective coupling [17]). Positioning the electron beam at the core of the Ag hemisphere-like head (figure 2(a), black curve), a broad maximum at ∼8.5 eV (∼146 nm) and a weaker maximum around ∼3.8 eV (∼326 nm) characteristic of the bulk plasmon excitations of

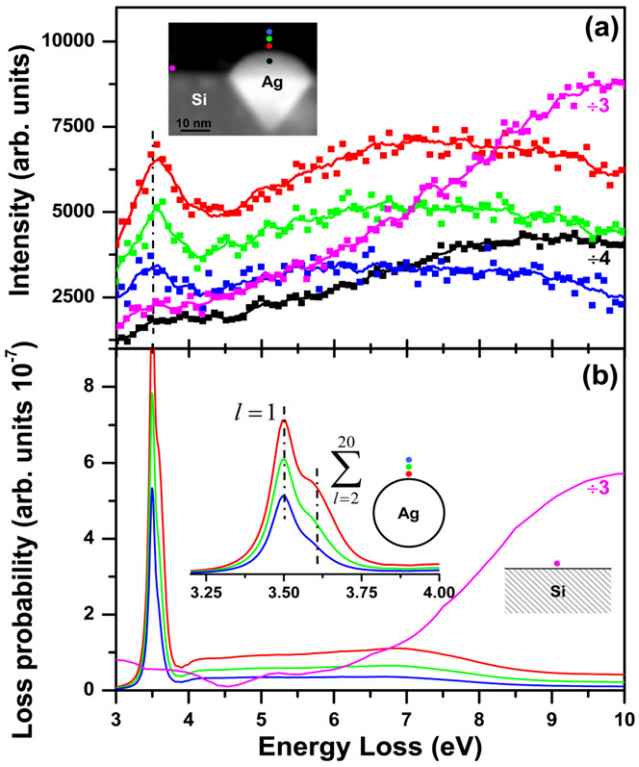

Figure 2. (a) The STEM-EELS spectra acquired at different locations of the Ag NP and the Si substrate schematized by color dots in the inset. All spectra were first aligned and normalized to the ZLP of the red curve (i.e. that at 1 nm from the Ag NP surface), and the ZLPs were then deconvoluted from the spectra. The spectrum taken at 1 nm from the surface of Si (∼20 nm from the edge of the NP; purple curve) and that taken at the core of the Ag NP (black curve) were divided by 3 and 4, respectively, to fit into the scale of the figure. Green (blue) curve, the spectrum acquired at 3 (6) nm from the Ag NP surface. (b) The calculated impact-parameter dependent STEM-EELS spectra for an individual Ag nanosphere (radius, 15 nm) and an Si film. The insets show an enlargement of the region below 4.0 eV and the geometrical constraints used for the calculations. Each impact parameter used in the calculation is identical to that of its experimental counterpart in (a). The purple curve was divided by 3 to fit into the scale of the figure.

Ag were observed [28]. Further positioning the electron beam at an impact parameter of 1 nm from the NP surface (similar to optical near-field setup and propitious for the coupling to surface excitations [21]; figure 2(a), red curve), we observed the prominent SP resonance of Ag around ∼3.5 eV (∼355 nm), in good agreement with the reported value for hemispherical Ag NPs [27]. Nevertheless, a broad surface excitation was also revealed at ∼7 eV (∼177 nm; figure 2(a), red curve), where the real part of the complex dielectric function of Ag is still negative [26, 28], suggesting its SP character [21]. With the further increase in impact parameters for STEM-EELS probing (figure 2(a); 3 nm, green curve; 6 nm, blue curve), the SP excitation around ∼3.5 eV appears to gently red-shift and is accompanied with a separate red-shift of nearly 1 eV for the broad spectral intensity at ∼7 eV.

In *spherical* NPs, an impact-parameter dependent red-shift of surface excitations, such as that observed in figure 2(a), is well known to arise from the frequency-dependent multipolar polarizability $\alpha_l(\omega)$ of the NP and can be expressed as the equation below in the non-retarded, electrostatic limit that does not consider the SP dispersion in momentum space [24].

$$\alpha_l(\omega) = \frac{l[\varepsilon(\omega) - \varepsilon_{\rm m}(\omega)]}{l\varepsilon(\omega) + (l+1)\varepsilon_{\rm m}(\omega)} a^3$$

where $\varepsilon(\omega)$ and $\varepsilon_{\rm m}(\omega)$ are the respective complex dielectric functions of the NP and the bound medium (vacuum here, $\varepsilon_{\rm m} = 1$), a is the radius of the NP, and l is the mode quantum number ($l = 1$, dipole mode; $l = 2$, quadruple mode; etc.). The surface-excitation energy $\hbar\omega$ ($\hbar = h/2\pi$; h, the Planck's constant) taking place at the divergence of $\mathrm{Im}\{\alpha_l(\omega)\}$ evolves with the increase in l [24], while the near-field extension of the given l mode into free space inversely scales with the energy as v/ω (v, the electron velocity; $0.7c$ at 200 kV; c, the speed of light) [21, 29]. This near-field scaling thus suggests that a large impact parameter would favor a surface excitation with a lower eigenenergy due to its larger v/ω, giving rise to the impact-parameter dependent red-shift of the surface spectral features [21]. In hemispherical or supported spherical objects with non-conducting substrates (such as Si here) [30, 31], the thorough numerical STEM-EELS investigations considering all multipolar components have indicated that probing the objects at their apical locations (i.e. red, green, and blue curves in figure 2(a)) can lead to surface excitations in resemblance to those of the bare spherical counterpart. We thus performed the non-retarded STEM-EELS calculations for bare Ag nanospheres using the impact-parameter dependent analytical equation on the basis of $\alpha_l(\omega)$ [24], which is computationally efficient compared to the lengthy numerical evaluations in [30, 31] and also faithfully catches the physics for the impact-parameter dependent red-shift and the related SP characteristics observed in the Ag NPs as demonstrated below.

Figure 2(b) shows the impact-parameter dependent STEM-EELS spectra calculated per unit path length along the electron trajectory for an Ag nanosphere ($a = 15$ nm, estimated from figure 1(a)) and an infinitely large Si film. For the Ag NP calculations, we have considered the contributions of high order l up to 20. Integrations of even higher order l do not lead to visible changes in the scale of the figure as a result of their negligible contributions to the currently rather small NP [24]. In addition, the criterion for the electrodynamics retardation, $a \cdot \omega/v > 1$ [29], is not fulfilled in the spectral range that we are interested in ($\lesssim$10 eV), justifying our exploitations of the non-retarded calculations for Ag NPs [24].

Comparing figures 2(a) and (b), it is obvious that the experimentally observed SP peak at ∼3.5 eV consists of a dominant dipolar SP component at 3.5 eV and contributions from all higher order modes (shoulder, 3.6 eV) as shown in the inset of figure 2(b). With the increase in impact parameters from 1 (red curve; figure 2(b), inset) to 6 nm (blue curve), the high order shoulder rapidly decays as a vanishing spectral feature due to the v/ω scaling, whereas the dipolar contribution remains as the predominant spectral feature. The energy resolution of our STEM-EELS instrument is, however, not sufficient to distinguish the two bands, only 0.1 eV apart (figure 2(b), inset). From experimental aspects, the summation

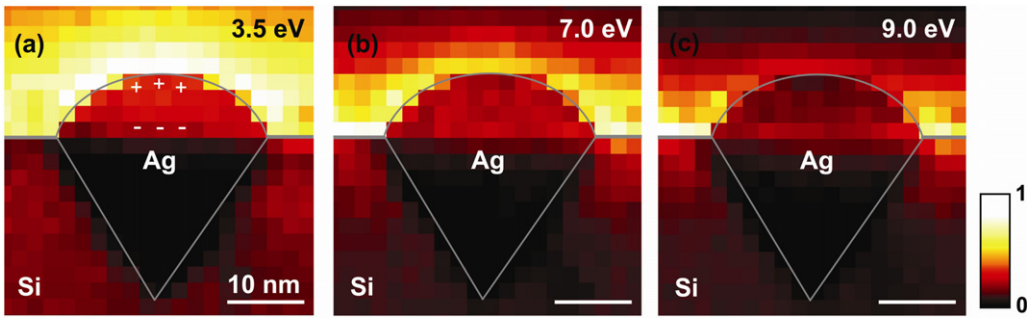

Figure 3. STEM-EELS mapping of (a) 3.5 eV, (b) 7.0 eV, and (c) 9.0 eV surface resonances in the material with the contrast maxima signifying the most prominent excitation locations for the given spectral features. The positive and negative signs in (a) denote the dominant dipolar character of the near-field features. The mesh dimension is 2 nm × 2 nm, and the Ag NP and Si surfaces are outlined by gray lines. Color scale bar, the linearly normalized image contrast.

of both bands then leads to a gently blue-shifted SP feature from 3.5 eV at the impact parameter of 1 nm (figure 2(a), red curve). Upon increased impact parameters, the predominant excitations for the dipolar SP at 3.5 eV (figure 2(b), inset) could account for the slight red-shift to 3.5 eV in figure 2(a) (green and blue curves). In the calculations shown in figure 2(b), the spectral red-shift of the ∼7 eV excitation to ∼5–6 eV arising from the impact-parameter dependent excitations of the SP multipolar components was also revealed, consistent with figure 2(a). Indeed, the agreement between experiments, figure 2(a), and calculations, figure 2(b), for the Ag NPs is satisfactory and establishes the SP multipolar nature for the surface excitations, ∼3.5 and ∼7.0 eV, in the ultra-violet regime. The calculations on the basis of a spherical NP, though simple, unveil the origin for the impact-parameter dependent spectral red-shift in figure 2(a). Nevertheless, the Ag NP calculations appear to under-estimate the broad spectral intensities near ∼7 eV, possibly due to effects of the Si substrate. For further inspections, we then performed impact-parameter dependent calculations for the Si film (1 nm from the surface; figure 2(b), purple curve) [22]. The calculation shows a good agreement with the experiment (figures 2(a) and (b), purple curve), and Si actually displays appreciable surface contributions above ∼6 eV. This later characteristic may contribute to the intense surface feature of Ag NPs near ∼7 eV (figure 2(a)), while an unambiguous determination of its origin requires more realistic calculations taking into account the actual sample geometry, which is beyond the scope of this work. In figure 2(b), the calculated broad spectral features below ∼4 eV for Si (purple curve) result from Cherenkov radiation (CR) that couples marginally to SPs [32] and their correlations with SPs in the Ag NPs can thus be ignored. Compared to the prominent CR excitations for an infinitely thick Si in figure 2(b), the vanishing experimental CR features in figure 2(a) should arise from the relatively small thickness of Si (∼70 nm, along the beam incident direction) considering that the CR excitation probability is proportional to the material thickness [32]. This characteristic reinforces the negligible role played by CR in the SP features of Ag NPs mentioned above.

Figures 3(a)–(c) illustrate the STEM-EELS mapping of the spectral features at 3.5, 7.0, and 9.0 eV (∼138 nm), respectively. The spectral mapping was performed by rastering the electron beam on the material in a mesh by mesh manner (2 × 2 nm per mesh) [8, 21, 23]. After aligning ZLPs acquired at each mesh, the spectral amplitudes of the given surface excitations were then used to map out their respective spatial distributions [8, 21, 23]. It has been well established that the STEM-EELS mapping nicely mimics the electric near-field distributions of the surface excitations, in particular, the near-field enhancements at local geometrical constraints that are rather invisible to optical approaches due to the limited spatial resolution [21, 33].

In the STEM-EELS map of the 3.5 eV SP, figure 3(a), the contrast maximum localized at the top of the Ag NP is characteristic of a dipole-like near-field behavior (see the schematic positive and negative signs) [6], in perfect consistency with the determination of the dipolar SP nature at 3.5 eV, figure 2. Moreover, such a contrast-maximum feature, figure 3(a), is representative of the local SP near-field enhancements [6, 21, 33] and might thus be of practical interest for future plasmonics and SERS applications. At 7.0 eV, figure 3(b), the surface of the Ag NP is imaged by sharp contrasts as expected for surface excitations like those in figure 3(a), evidencing again the SP character of this peak. In figure 3(b), the contrast maxima are, however, localized on the Si surface, signifying the aforementioned appreciable Si contributions above ∼6 eV, figure 2. At 9.0 eV, the surface excitations of Si dominate over those of Ag as shown in figure 2, and the corresponding spectral mapping indeed faithfully reflects the contrast maxima on the Si surface, figure 3(c). The spatial resolving power established in the above STEM-EELS mapping is superb considering that state-of-the-art nanoprobe-based SNOM could not resolve the field distribution around the Ag NP beyond its spatial resolution (a few tens of nanometers) [33] and, more importantly, the introduced electromagnetic interaction between its nanoprobe and the plasmonic entity could interfere with the physical interpretation [20]. It should also be pointed out that the contrast delocalization into vacuum in figure 3 represents the near-field extension into free space for the surface excitations (proportional to v/ω) [21] and decreases with the increasing surface-excitation energy as expected.

4. Conclusion

In summary, the spatially resolved investigation of the SP characteristics in individual Ag NPs (∼30 nm) in the ultraviolet spectral regime has been achieved using STEM-EELS. The NP shows a prominent SP resonance at ∼3.5 eV (∼355 nm) and a broad SP at ∼7.0 eV (∼177 nm), both of which are in good agreement with the associated STEM-EELS calculations. STEM-EELS mapping was further performed to unveil the spatial distributions of these SPs, and the dipolar near-field characteristics with remarkable field enhancements imaged for the 3.5 eV SP at one end of the NP could be of practical use for plasmonics and ultra-sensitive sensing by SERS.

Acknowledgments

This work was supported by the National Taiwan University Excellence Project and the National Science Council of Taiwan. One of the authors, Pradeep Sharma, wishes to acknowledge financial support from Taiwan International Graduate Program of Academia Sinica, Taiwan.

References

[1] Raether H 1980 *Excitation of Plasmons and Interband Transitions by Electrons* (*Springer Tracts in Modern Physics* vol 88) (Berlin: Springer)
[2] Ritchie R H 1957 *Phys. Rev.* **106** 874
[3] Stern E A and Ferrell R A 1960 *Phys. Rev.* **120** 130
[4] Schwerdtfeger P 2003 *Angew. Chem. Int. Edn* **42** 1892
[5] Aizpurua J, Bryant G W, Richter L J and García de Abajo F J 2005 *Phys. Rev.* B **71** 235420
[6] Romero I, Aizpurua J, Bryant G W and García de Abajo F J 2006 *Opt. Express* **14** 9988
[7] Nordlander P, Oubre C, Prodan E, Li K and Stockman M I 2004 *Nano Lett.* **4** 899
[8] Nelayah J, Kociak M, Stéphan O, García de Abajo F J, Tencé M, Henrard L, Taverna D, Pastoriza-Santos I, Liz-Marzán L M and Colliex C 2007 *Nat. Phys.* **3** 348
[9] Aizpurua J, Hanarp P, Sutherland D S, Käll M, Bryant G W and García de Abajo F J 2003 *Phys. Rev. Lett.* **90** 057401
[10] Hao F, Nehl C L, Hafner J H and Nordlander P 2007 *Nano Lett.* **7** 729
[11] Canfield B K, Husu H, Laukkanen J, Bai B, Kuittinen M, Turunen J and Kauranen M 2007 *Nano Lett.* **7** 1251
[12] Klar T, Perner M, Grosse S, von Plessen G, Spirkl W and Feldmann J 1998 *Phys. Rev. Lett.* **80** 4249
[13] Kneip K, Moskovits M and Kneipp H 2006 *Surface-Enhanced Raman Scattering: Physics and Applications* (Berlin: Springer)
[14] Atay T, Song J-H and Nurmikko A V 2004 *Nano Lett.* **4** 1627
[15] Khan I, Cunningham D, Lazar S, Graham D, Smith W E and McComb D W 2006 *Faraday Discuss.* **132** 171
[16] Danckwerts M and Novotny L 2007 *Phys. Rev. Lett.* **98** 026104
[17] Biring S, Wang H-H, Wang J-K and Wang Y-L 2008 *Opt. Express* **16** 15312
[18] Ozbay E 2006 *Science* **311** 189
[19] Wang H-H, Liu C-Y, Wu S-B, Liu N-W, Peng C-Y, Chan T-H, Hsu C-F, Wang J-K and Wang Y-L 2006 *Adv. Mater.* **18** 491
[20] Chu J-Y, Wang T-J, Chang Y-C, Lu Y-J, Lin M-W, Yeh J-T and Wang J-K 2008 *Ultramicroscopy* **108** 314
[21] Chu M-W, Chen C H, García de Abajo F J, Deng J-P and Mou C-Y 2008 *Phys. Rev.* B **77** 245402
Chu M-W, Myroshnychenko V, Chen C H, Deng J-P, Mou C-Y and García de Abajo F J 2009 *Nano Lett.* **9** 399
[22] Moreau P, Brun N, Walsh C A, Colliex C and Howie A 1997 *Phys. Rev.* B **56** 6774
[23] Bosman M, Keast V J, Watanabe M, Maaroof A I and Cortie M B 2007 *Nanotechnology* **18** 165505
[24] Ferrell T L and Echenique P M 1985 *Phys. Rev. Lett.* **55** 1526
[25] Sharma P, Liu C Y, Hsu C-F, Liu N W and Wang Y L 2006 *Appl. Phys. Lett.* **89** 163110
[26] Palik E D (ed) 1985 *Handbook of Optical Dielectric Constants of Solid* (San Diego, CA: Academic)
[27] Ouyang F, Batson P E and Isaacson M 1992 *Phys. Rev.* B **46** 15421
[28] Schlüter M 1972 *Z. Phys.* **250** 87
[29] García de Abajo F J and Howie A 2002 *Phys. Rev.* B **65** 115418
[30] Aizpurua J, Rivacoba A and Apell S P 1996 *Phys. Rev.* B **54** 2091
[31] Zabala N and Rivacoba A 1993 *Phys. Rev.* B **48** 14534
[32] Chen C H, Silcox J and Vincent R 1975 *Phys. Rev.* B **12** 64
[33] Myroshnychenko V, Rodríquez-Fernández J, Pastoriza-Santos I, Funston A M, Novo C, Mulvaney P, Liz-Marzán L M and García de Abajo F J 2008 *Chem. Soc. Rev.* **37** 1792